PCCP

ROYAL SOCIETY OF CHEMISTRY

PAPER

Cite this: *Phys. Chem. Chem. Phys.*, 2021, **23**, 8292

Resolving the F_2 bond energy discrepancy using coincidence ion pair production (cipp) spectroscopy†

Kristján Matthíasson, [a] Ágúst Kvaran, *[a] Gustavo A. Garcia, [b] Peter Weidner [c] and Bálint Sztáray *[c]

Received 31st December 2020,
Accepted 5th March 2021

DOI: 10.1039/d1cp00140j

rsc.li/pccp

Coincidence ion pair production (cipp) spectra of F_2 were recorded on the DELICIOUS III coincidence spectrometer in the one-photon excitation region of 125 975–126 210 cm^{-1}. The $F^+ + F^-$ signal shows a rotational band head structure, corresponding to F_2 Rydberg states crossing over to the ion pair production surface. Spectral simulation and quantum defect analysis allowed the characterization of five new molecular Rydberg states (F_2**): one Π and four Σ states. The lowest-energy Rydberg state spectrum observed (T_0 = 125 999 cm^{-1}) lacked some of the predicted rotational structure, which allowed an accurate determination of the ion pair production threshold of $15.6229_4 \pm 0.0004_3$ eV. Using the well-known atomic fluorine ionization energy and electron affinity, this number leads to a ground state F–F dissociation energy of $1.6012_9 \pm 0.0004_4$ eV. Photoelectron photoion coincidence (PEPICO) experiments were also carried out on F_2 and the dissociative photoionization threshold to $F^+ + F$ was determined as 19.0242 ± 0.0006 eV. Using the atomic fluorine ionization energy, this can be converted to an F_2 dissociation energy of $1.6013_2 \pm 0.0006_2$ eV, further confirming the cipp-derived value above. Because the two experiments were independently energy-calibrated, they can be averaged to $1.6013_0 \pm 0.0003_6$ eV and this value can be used to derive the fluorine atom's 0 K heat of formation as $77.25_1 \pm 0.01_7$ kJ mol^{-1}. This latter is in excellent agreement with the latest Active Thermochemical Table (ATcT) value but improves its accuracy by almost a factor of three.

1 Introduction

Of the halogen molecules F_2, Cl_2, Br_2, and I_2, the photoexcitation dynamics and spectroscopy relevant to electronic excitations in the Rydberg states energy region are least studied for fluorine, F_2. Rydberg states of fluorine have been investigated by absorption spectroscopy,[1–3] photoionization mass spectrometry,[4,5] electron energy-loss spectroscopy,[6–8] photoelectron spectroscopy,[9–11] threshold photoelectron spectroscopy,[12] resonance-enhanced multiphoton ionization spectroscopy,[13] and theoretically.[7,14] Ion-pair states are also known to play an important role in that energy region.[14–16]

Interactions between Rydberg and ion-pair states are well known from studies of other halogen[17–21] and interhalogen[22–24] molecules. These have been found to occur either above[17,18] or below[19–21] the dissociation energy thresholds for halogen ion-pair molecular states. Exciting F_2 into a bound high energy Rydberg state which interacts with an ion-pair state should, therefore, simultaneously form positive and negative ions, F^+ and F^- at discreet energies, once the excitation energy goes above that of the ion pair production threshold.[15,16] Experimentally, various avenues have been explored to determine the ion pair production threshold energy. Hepburn and co-workers developed threshold ion pair production spectroscopy (TIPPS), (which is analogous to PFI-ZEKE or MATI spectroscopy)[25,26] where they excited the neutral molecule to a highly excited state, just below the ion pair production threshold E_{tipp} and use a pulsed field to produce the ion pair.[27] Like in MATI, discrimination against the prompt ion is achieved by using a small DC field and after a short delay, an opposite field is used for field ion pair production. In their experiments, only the positive ions were detected and mass analyzed. More recently, Yang *et al.* utilized velocity map imaging (VMI) of the positive ions by using a laser that was tuned to an energy less than 100 meV above the ion pair production threshold and the E_{tipp} was determined from the fragment ion velocities.[15,16] In both experiments, the electric field dependence of the dissociation threshold was studied and, similar to PFI-ZEKE, shifts proportional to the square root of the field were observed.

[a] *Science Institute, University of Iceland, Dunhagi 3, Reykjavík 107, Iceland. E-mail: agust@hi.is*
[b] *Synchrotron SOLEIL, L'Orme des Merisiers, St. Aubin BP 48, Gif sur Yvette 91192, France*
[c] *Department of Chemistry, University of the Pacific, Stockton, CA-95211, USA. E-mail: bsztaray@pacific.edu*

† Electronic supplementary information (ESI) available: Argon lines used for absolute energy calibration. See DOI: 10.1039/d1cp00140j

While in both of these experiments only the positive ion was detected, Marggi Poullain *et al.* detected both particles, NO^+ and O^- from NO_2, by using coincident momentum spectroscopy on a double-velocity spectrometer coupled to the DESIRS VUV beamline of the Soleil synchrotron, operating in a single-bunch mode. From these experiments, they determined kinetic energy release (KER) and ion fragment angular distribution functions.[28]

In this paper, we present the first data from a new continuous coincidence ion pair production (cipp) spectroscopy experiment, which is analogous to modern synchrotron-based, imaging photoelectron photoion coincidence (PEPICO) spectroscopy, except for ion pair detection. The experiment utilized one-photon excitation, together with continuous molecular beam inlet, velocity map imaging setup for the anions, and the modified Wiley–McLaren time-of-flight 3D momentum imaging ion mass analyzer for the positive ions.[29] Continuous coincidence detection of both particles of the F^+–F^- ion pairs means very low background below the ionization energy and, due to the high photon energy resolution of the VUV source, it allowed detailed identification and characterization of five new Rydberg states, which cross over to the ion-pair surface. Simulation analysis of the spectral structures allows very accurate determination of the ion pair production threshold energy, from which the most accurate value of the F_2 dissociation energy was determined. Furthermore, because the cipp experiments utilized the existing DELICIOUS III double-imaging PEPICO setup,[29] dissociative photoionization (PEPICO) experiments were also carried out for an independent determination of the same F_2 dissociation energy.

2 Experimental

The experiments were carried out with the DELICIOUS III double-imaging photoelectron photoion coincidence (i^2PEPICO) spectrometer on the DESIRS undulator beamline of Synchrotron Soleil, in France. The instrument has been described in detail elsewhere[29] and only a brief summary of the relevant parts is given here. Briefly, molecular fluorine was entered into the ionization chamber through a supersonic expansion of a 5% F_2 in He mixture, collimated with the double skimmer setup of the SAPHIRS molecular beam end station. Photons from the variable polarization undulator OPHELIE2 were dispersed by a 6.65 m normal-incidence monochromator with a 2400 lines per mm grating and focused onto a 200/70 μm (H/V) spot in the ionization region. The entrance and exit slits of the monochromator were set to 50 μm, providing an energy resolution of 0.6 meV at 16 eV. To block out high-order harmonics, a gas filter located upstream of the beamline was filled with neon at around the dissociative photoionization and with argon near the ion pair production energy region. Several well-known Rydberg absorption lines for these gases, corresponding to dips in the ion signal, were used for calibration (see Table S1, ESI†). The DELICIOUS III spectrometer comprised of an electron velocity map imaging setup and a modified Wiley–McLaren time-of-flight 3D momentum imaging ion mass analyzer in a multistart–multistop coincidence detection mode. This setup produces a multi-dimensional coincidence data set, two cross sections of which yield photoion mass-selected photoelectron spectra, as well as mass spectra of internal energy-selected photoions. In the new coincidence ion pair production (cipp) experiments, the same physical setup was utilized, except that anions were detected on the imaging electron detector, in coincidence with cations from the same ion pair production events. In the PEPICO setup, electrons arrive only nanoseconds after the ionization event, providing the start signals for the electron/ion coincidences. Photoions arrive several microseconds later and the time differences between the start and stop signals correspond very closely to the photoion TOFs. However, in the cipp experiments, the cation actually arrives faster, due to the larger electric fields in the ion analyzer, and was used as the start signal in the coincidence acquisition. Therefore, ion pair production coincidences were registered at the calculated and experimentally confirmed time delay between the F^- and F^+ ions, using raytracing simulations of the DELICIOUS III coincidence setup.

Because the typical fwhm of the cipp spectral peaks is less than 1 meV, very accurate absolute photon energy calibration was necessary in this photon energy range. Serendipitously, multiple lines in the argon Rydberg progression happen to fall directly into the energy range of our cipp spectra. Several argon absorption scans were recorded in this energy range and the argon lines that were used for calibration are listed in Table S1 in the ESI.†[30–32] For the dissociative photoionization (PEPICO) experiments, the absolute photon energy calibration was carried out with neon in the gas filter, using the $2p^5(^2P^\circ_{3/2})4s\ ^2[3/2]^\circ$ and $2p^5(^2P^\circ_{3/2})3d\ ^2[1/2]^\circ$ $J = 1$ lines at 19.6882 eV and 20.0264 eV, respectively.[32,33]

3 Results and analysis

3.1 Spectra analysis

The coincidence ion pair production experiments were carried out in an electric field (E) and, as previously noted,[15,16] the cipp lines show a field-dependent red shift. The Stark-shift is usually given as $\alpha\sqrt{E(\mathrm{V\ cm^{-1}})}\ (\mathrm{cm^{-1}})$ where typical measured values of α range from -3.9 to -6.11.[27] Yang *et al.*,[16] however, determined an α factor of -1.1 in the zero-field extrapolation of the ion pair production threshold (E_{tipp}). In their experiments, they used velocity map imaging with a fixed photon energy of 15.715 eV, at more than 700 $\mathrm{cm^{-1}}$ above E_{tipp}. We recorded the cipp spectra at four different electric fields, at 17.7, 30.2, 46.1, and 65.6 V $\mathrm{cm^{-1}}$ and used these spectra to extrapolate to zero field. We have found that, while the red-shift of the cipp lines indeed follows the square-root formula, the factor is energy-dependent between -0.96 $\mathrm{cm^{-1}}$ at threshold and -1.7 $\mathrm{cm^{-1}}$ at 15.64 eV. This might be because Rydberg states are affected differently by the Stark shift, as noted in other atomic and molecular systems, with the higher n states being more susceptible to the electric field.[34] Therefore, we used an energy-dependent extrapolation formula to correct the four cipp spectra for the electric field effect. The resulting four

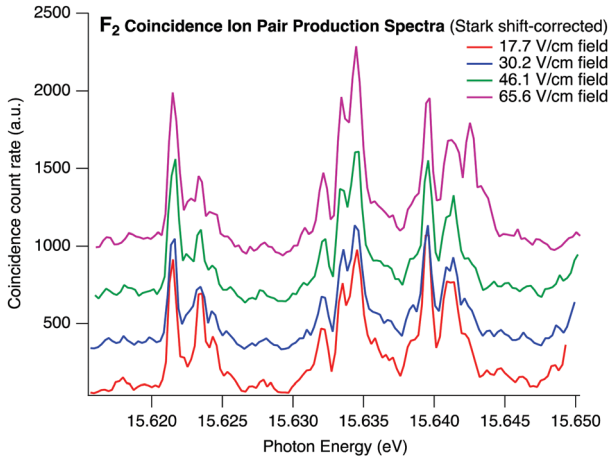

Fig. 1 Coincidence ion pair production (cipp) spectra in four different electric fields, after extrapolation to zero-field.

spectra are shown in Fig. 1. While within the energy resolution of our data, the four spectra look very similar, the intensities do show some electric field dependence. Most notably, a shoulder peak at 15.643 eV shows a significant enhancement in the highest-field (65.6 V cm^{-1}) cipp spectrum, most likely corresponding to the $^1\Sigma_u^+[3/2]\ 16p\pi_u$ ($v' = 0, J' = 6$) level (*vide infra*).

The lowest-field (17.7 V cm^{-1}) spectrum was used for spectral simulation. The experimental spectrum along with the calculated spectrum is shown in Fig. 2, for the region of 125 950–126 210 cm^{-1} (15.616–15.650 eV). No coincidence signal was detectable at lower photon energies, which is in line with the expected value of the F^+/F^- ion pair production threshold.[35]

Most of the spectral structure could be simulated quite well with PGOPHER[36] by assuming the rotational structure due to one-photon transitions from the F_2 ground state $X^1\Sigma_g^+$, $v' = 0$ to a total of five, partly overlapping Rydberg states (see Fig. 2). Some weak structures, in the region of 126 050 cm^{-1} in particular, were left unassigned. The spectral structure, in terms of

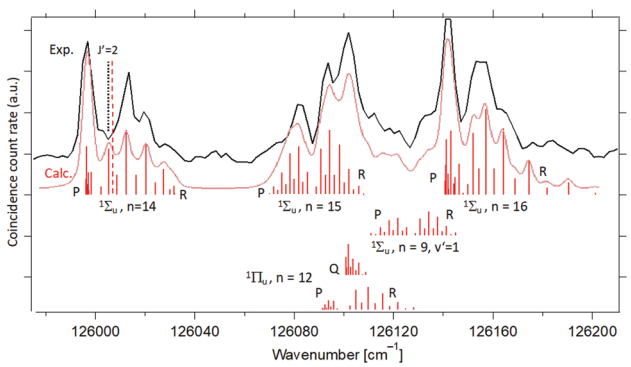

Fig. 2 F_2 coincidence ion pair production spectra in the 125 950–126 210 cm^{-1} photon energy region. Experimental spectrum (black), calculated spectrum (red) using 5 cm^{-1} linewidths, and rotational lines (red sticks). The ion pair threshold is indicated by a red dashed line. $J' = 2$ for the $^1\Sigma_u^+[3/2]14p\pi_u$ state is indicated by a dashed black line. Assignments for the spectral contributions are indicated.

rotational line series, allowed identification of transitions to four Σ states (P and R lines only) and one Π state (P, Q and R lines). These are labelled as $^1\Sigma_u$ and $^1\Pi_u$ states, respectively. The Rydberg state spectra were simulated by using the symmetric top approximation. The best fit was obtained with a Boltzmann distribution corresponding to a rotational temperature of about 35 K and rotational line widths of 5 cm^{-1}. A critical parameter in the simulation procedure, in order to derive satisfactory structure fit, was the relative degeneracy due to nuclear statistics, which for F_2 with nuclear spin 1/2 corresponds to an odd J'' : even J'' ratio of 3 : 1.[37] While peak positions of experimental and calculated spectra match quite well, there is some discrepancy in the relative intensities of the spectral structure. This is not surprising, considering that the calculation assumes absorption only and does not take into account intersystem crossing from the excited Rydberg states to ion-pair state(s) surface(s), which are energy-level and even electric-field dependent. Furthermore, because the temperature used in the simulation depends on the relative intensities, its value of 35 K is not necessarily reliable. Spectroscopic parameters derived from the simulation are listed in Table 1. Some scattered values of rotational constants observed could be an indication of perturbation effects due to state mixing. Further characterization of the observed states was achieved by quantum defect analysis.

3.2 Quantum defect analysis

The band origin (v^0) of a Rydberg state (F_2**) spectrum can, to a first approximation, be expressed as,

$$v^0([\Omega_c]nl\lambda) = \mathrm{IE}([\Omega_c, v]) - \frac{R_\infty}{(n-\delta_l)^2} \qquad (1)$$

where $[\Omega_c]nl\lambda$ refers to a Rydberg state which converges to either of the two spin–orbit components $\left(\Omega_c = \frac{3}{2}, \frac{1}{2}\right)$ of the ground ionic state $F_2^+(X^2\Pi_g)$ at vibrational level v, for a Rydberg electron with principal quantum number n, in a molecular orbital λ, corresponding to an atomic orbital l. IE($[\Omega_c,v]$) is the ionization energy of $F_2(X^1\Sigma_g^+(v'' = 0, J'' = 0))$ to form F_2^+ ($[\Omega_c,v]$). R_∞ is the Rydberg constant (109 735.85 cm^{-1}) and δ_l is an

Table 1 Rydberg state specifications ($^{2\Sigma+1}X[\Omega_c]nl\lambda$ for $^{2\Sigma+1}X$ = term symbol for the Rydberg state) vibrational quantum numbers (v'), band origin (v^0) and rotational parameters (B', D') based on spectra simulation shown in Fig. 2 and quantum defect analysis shown in Fig. 3. See also main text

State assignments	v'	Band origin (v^0) [cm^{-1}]	B_e' [cm^{-1}][a]	D_e' [cm^{-1}][a]
$^1\Sigma_u^+[3/2]14p\pi_u$	0	125 999	1.18 ± 0.01	0.0015 ± 0.0003
$^1\Sigma_u^+[3/2]15p\pi_u$	0	126 086	0.9 ± 0.1	(0)
$^1\Pi_u[1/2]12p\sigma_u$	0	126 099	1 ± 0.1	(0.0002)
$^1\Sigma_u^+[3/2]9p\pi_u$	1	126 126	0.9 ± 0.1	(0)
$^1\Sigma_u^+[3/2]16p\pi_u$	0	126 147	0.96 ± 0.1	(−0.0014)

[a] Precision of parameters is affected by overlap of spectra and rotational line overlaps.

l-dependent quantum defect value, which is a measure of how much a Rydberg series diverges from the corresponding hydrogen atom Rydberg series. A δ_l value of about 0.70 ± 0.05 has been reported for the p(l = 1) Rydberg series of F_2.[1] Judging from atomic energy levels,[32] δ_l values of about 1.23, 0.77 and 0.0 are found for s(l = 0), p(1) and d(2) Rydberg electron orbitals of the fluorine atom. By matching observed band origins of Rydberg state spectra and the corresponding values calculated by eqn (1) for given ionization energies and n the δ_l were derived. The band origin of the Σ and Π Rydberg states observed (*vide supra*) along with those of lower energy spectra reported by Gole and Margrave[1] could be made to fit eqn (1) for two Rydberg electron series, converging to the $\Omega_c = \frac{3}{2}$ and $\frac{1}{2}$ states, respectively (see Fig. 2 and 3). This was achieved by using a common δ_l value of 0.70 ± 0.04, which strongly suggests that these correspond to np Rydberg orbitals (npπ_u for the Σ states and npσ_u for the Π states; see Table 1).

3.3 Ion pair production threshold

One of the key features of the simulation is the apparent lack of the J' = 2 rotational peak in the first Σ state experimental spectrum (at around 126 000 cm^{-1}). This peak, which should occur at 126 004 cm^{-1} (see Fig. 2) must be missing because its excited state energy level is below the ion pair production threshold. This finding allows us to estimate, with high certainty, the $F_2 \rightarrow F^+ + F^-$ dissociation threshold, which can also be used to determine the F–F bond dissociation energy, $D_0(F_2)$. The energies (E) of the rotational levels J' = 2 and J' = 3 of the $^1\Sigma_u^+$ 14pπ_u state, converging to the $^2\Pi_g$[3/2] ground state of F_2^+ are,

$$E(^1\Sigma_u^+[3/2]\ 14p\pi_u\ (v' = 0, J' = 2)) = 126\,004\ cm^{-1} = 15.6225\ eV$$

$$E(^1\Sigma_u^+[3/2]\ 14p\pi_u\ (v' = 0, J' = 3)) = 126\,011\ cm^{-1} = 15.6234\ eV$$

A final point of interest concerns the bandwidth and excited state lifetime. The simulation used the same bandwidth of 5 cm^{-1} for all spectral lines. However, to determine lifetimes from this bandwidth, much higher photon resolution would be needed, such as the one available at the FTS branch in DESIRS.[48]

3.4 Dissociative photoionization (PEPICO)

Imaging PEPICO experiments were carried out for the $F_2 \rightarrow F_2^+ + e^- \rightarrow F^+ + F + e^-$ dissociative photoionization process between 18.96 and 19.04 eV photon energy. In this range, the fractional abundance of the F_2^+ parent ion gradually decreases with a crossover at 19.022 eV and a sharp disappearance at 19.025 eV. The fractional abundances as a function of the photon energy (*i.e.*, the breakdown curves) are shown in Fig. 4. In order to take into account the contamination of the threshold electron signal with energetic electrons in the coincidence spectra, the hot-electron subtraction scheme of Sztáray and Baer was applied.[38] Briefly, the signal from a conveniently chosen ring area, surrounding the central spot of the threshold electrons, was subtracted from the central photoelectron signal, before it was multiplied by a factor that roughly corresponds to the detector area ratios between the centre and the ring regions. Furthermore, the effective kinetic energy (KE) resolution of the imaging detector was explored by using various radii for the centre region. Fig. 5 shows the breakdown curves with three different threshold electron KE resolutions. Each of these spectra were then independently analysed to

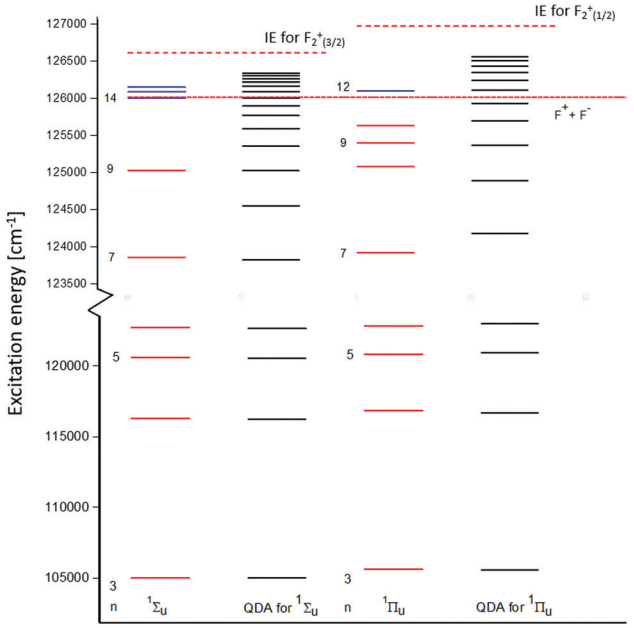

Fig. 3 Results of the quantum defect analysis. Calculated band origins (QDA in the figure) using eqn (1) matched to the previously determined band origins by Gole and Margrave (in red)[1] and those measured in this work (blue).

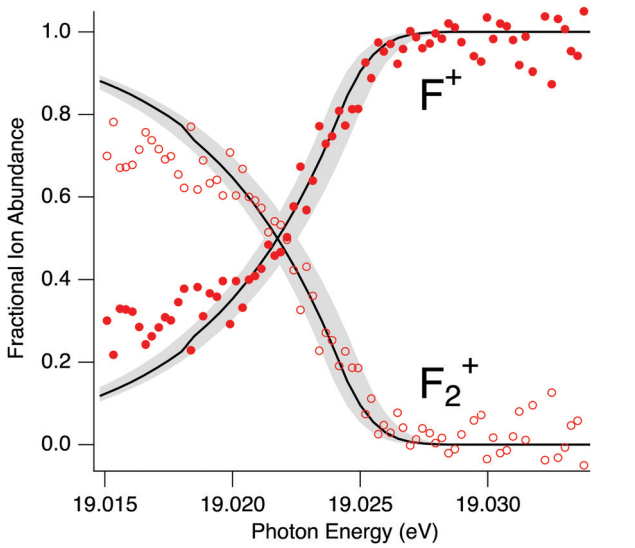

Fig. 4 Breakdown curves of the imaging PEPICO experiments on molecular fluorine. Dots and circles of gules show the experimental ion abundances. Solid lines show the best-fit results of the statistical thermodynamics model, and the shaded areas indicate the confidence intervals corresponding to the error bars in the 0 K appearance energy (E_0).

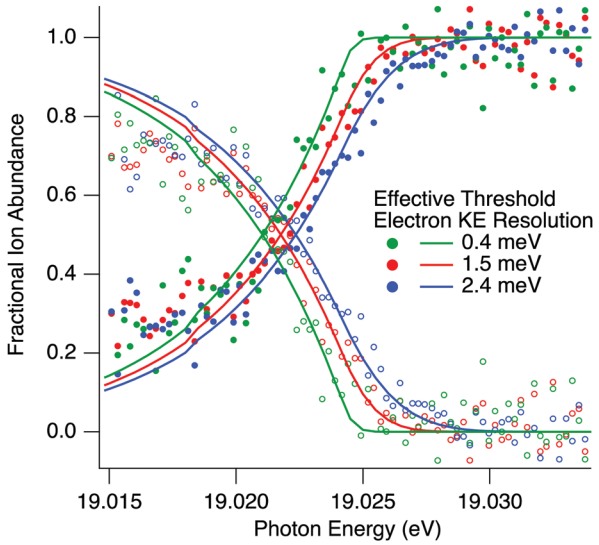

Fig. 5 Breakdown curves at three different threshold electron KE resolutions. Coloured dots and circles show the experimental ion abundances and solid lines show the model.

derive the 0 K dissociative photoionization appearance energies, taking the effective kinetic energy resolution into account.

The PEPICO breakdown curves were modelled as described by Sztáray *et al.*[39] Briefly, the internal energy distribution of the F_2 neutral precursor was calculated in the two-dimensional rigid-rotor approximation. This internal energy distribution was shifted by the difference of the photon energy and the F_2 adiabatic ionization energy (15.6946 ± 0.0001 eV),[15] then convolved with the experimental photon energy distribution and the threshold photoelectron kinetic energy resolution (modelled as a half Gaussian function) to yield the internal energy distribution of the F_2^+ molecular ion. Because the dissociation is fast on the time scale of the PEPICO experiment, integrating this energy distribution from the 0 K appearance energy (E_0) directly yields the breakdown curve. To obtain this latter value, the modelled curves were fitted to the experimental breakdown curves by varying the E_0 in the model. The solid lines in Fig. 4 and 5 show the modelling results with the best-fit value of E_0 = 19.0242 ± 0.0006 eV.

4 Discussion

4.1 Spectroscopy

In traditional absorption spectroscopic methods, typically it becomes gradually more difficult to resolve discreet rotational and vibrational spectra as the excitation energy closes in on the ionization energy of molecules. This is, for the most part, due to a denser distribution of Rydberg states at high energy levels, in addition to increased state crossing into unbound states, resulting in near-continuous spectra. The nature of the coincidence ion pair production detection, which involves selectivity of Rydberg states detected can, on the other hand, simplify the spectral structure.

The ion-pair coincidence spectra obtained in this study are formed *via* one-photon excitation to bound high energy Rydberg states, followed by state crossing to ion-pair states above the dissociation limit and subsequent dissociation to form F^+ and F^- ions. This mechanism can be presented as:

$$F_2 + h\nu \rightarrow F_2^{**} \quad \text{One-photon excitation}$$

$$F_2^{**} \rightarrow F^+F^- \quad \text{Rydberg} \rightarrow \text{ion-pair state crossing}$$

$$F^+F^- \rightarrow F^+ + F^- \quad \text{Ion pair dissociation}$$

A similar state crossing mechanism has been reported for other diatomic halogens, hydrogen halides, and some polyatomic molecules.[40–43] Other means of ion formation can be excluded because coincident ion formation only gives a signal when F^+ and F^- ions are formed simultaneously.

The results of the simulation and quantum defect analysis show that the $^1\Sigma_u^+$ series converges towards the $^2\Pi_g[3/2]$ state and that the $^1\Pi_u$ series converges towards the $^2\Pi_g[1/2]$ state of F_2^+ for states of p Rydberg electrons (Fig. 2–4 and Table 1). Alternatively, the only Π state identified in our spectra (ν^0 = 126 099 cm^{-1}) could fit the $^1\Pi_u[3/2]np\sigma_u$ Rydberg series for n = 15. We, however, exclude this possibility, because no other Π state spectra, which should belong to that series (n = 14 and 16) are visible in the studied region. Generally, one might expect to observe more Rydberg state spectra in the close vicinity of the ionization limit, due to large density of states. In this context, the nature of the coincidence ion pair detection in comparison with standard absorption definitely helps. Thus, in addition to photon absorption, a crossing from the excited neutral states to ion-pair states is involved. This latter step involves further selectivity for ion pair formation, depending on the intersystem crossing probabilities. Requirements of homogeneous state interactions ($\Delta\Omega = 0$) and conservation of symmetry ($u \leftrightarrow u$) will be important in that step. Thus, for example, a lack of observation of spectra due to optically allowed transitions to $^1\Pi_u[3/2]np\sigma_u$ and $^1\Sigma_u^+[1/2]np\pi_u$ Rydberg states could be associated with different electron transfer to form the ion-pair electron configuration ($F^+F^-[\sigma_g\pi_u^4\pi_g^4\sigma_u]$) in the step of intersystem crossing, along with different photoabsorption probabilities.

Furthermore, our quantum defect analysis showed that the $^1\Sigma_u^+$ Rydberg series state, labelled by Gole and Margrave as n = 8 should be n = 9.

4.2 Thermochemistry

The fluorine atom's 0 K heat of formation is simply one-half of the dissociation energy of the fluorine molecule. Most thermochemical databases (*e.g.*, CODATA, NIST-JANAF, Gurvich's thermodynamic properties book, the JPL compendium, and Burcat's thermochemical tables) recommend 77.28 ± 0.30 kJ mol^{-1}, taken from the 1976 paper of Colbourn *et al.* on the dissociation energy of the fluorine molecule.[3] This value is consistent with the most recently published experimental results of 77.46 ± 0.05 kJ mol^{-1} by Yang[15,16] and 77.258 ± 0.048 kJ mol^{-1} listed in version 1.122p

of the Active thermochemical tables (ATcT)[44] (earlier published as 77.26 ± 0.06 kJ mol^{-1} by Stevens *et al.*[45]). The former value is derived from $D_0(F_2)$ = 1.6056 ± 0.0010 eV, obtained by measuring the ion pair production threshold of the fluorine molecule, combined with the well-known ionization energy and electron affinity of the fluorine atom. While both of these values are more accurate and consistent with Colbourn's earlier result, they are inconsistent with each other, considering that their difference (0.20 kJ mol^{-1}) is twice as large as the sum of their error bars (0.11 kJ mol^{-1}). This discrepancy motivated extensive theoretical work by Kállay and co-workers and their best theoretical estimate for $\Delta_f H_0^\circ$(F) obtained was 77.48 ± 0.24 kJ mol^{-1}.[46] While their confidence interval does cover the ATcT value, it is much more consistent with (and is even farther from the ATcT number than) the Yang *et al.* ion pair production experimental result. From our detailed analysis of the coincidence ion pair production spectroscopic results, using the aforementioned upper and lower limits as identified by the first detected J' = 3 and the first missing J' = 2 rotational levels of the $^1\Sigma_u^+$ 14pπ_u state, we can determine a definitive value for the F_2 dissociation energy and, therefore, the F atom heat of formation.

As shown above, the energies of the J' = 2 and J' = 3 rotational levels of the $^1\Sigma_u^+$ 14pπ_u state are 15.6225 eV and 15.6234 eV, respectively. This means that the ion pair production threshold energy for $F_2 \rightarrow F^+ + F^-$ can be given as $15.6229_4 \pm 0.0004_3$ eV. Using the F adiabatic ionization energy of 17.42283 ± 0.00005 eV[44] and its electron affinity of 3.401190 ± 0.000002 eV[44] this translates to the following $D_0(F_2)$ value:

$$D_0(F_2) = 15.62294 - 17.42283 + 3.40119 \text{ eV} = 1.6012_9 \pm 0.0004_4 \text{ eV}$$

As detailed earlier, the TPEPICO experiments gave a 0 K appearance energy of 19.0242 ± 0.0006 eV for $F_2 \rightarrow F^+ + F + e^-$. Using the F adiabatic ionization energy above, this translates to the following $D_0(F_2)$ value:

$$D_0(F_2) = 19.0242 - 17.42283 \text{ eV} = 1.6013_2 \pm 0.0006_2 \text{ eV}$$

As this 0 K dissociation energy value was independently determined (and independently calibrated, *vide supra*) from the coincidence ion pair production threshold value, these two dissociation energies can be combined into a weighted average of $1.6013_0 \pm 0.0003_6$ eV, further reducing the error bars. Because this value represents twice the 0 K heat of formation of the fluorine atom, it can be obtained as $\Delta_f H_{0\,K}(F) = 77.25_1 \pm 0.01_7$ kJ mol^{-1}. This value is in very good agreement with the 77.258 ± 0.048 kJ mol^{-1} ATcT value and improves its accuracy by almost a factor of three. Furthermore, because ATcT thermochemical values are derived from a vast network of individual thermochemical determinations, adding our cipp and TPEPICO threshold energies directly into the ATcT web yields a new $\Delta_f H_{0\,K}(F)$ value with even lower error bars. Preliminary results from running the cipp and PEPICO threshold values on top of the current developmental version of ATcT yield a network $\Delta_f H_{0\,K}(F)$ value of 77.253 ± 0.016 kJ mol^{-1} and move the provenance from highly dependent on theory to highly dependent on experiments (over 50% on the cipp and close to 30% on the TPEPICO thresholds).[47]

The question remains why the Yang *et al.*[15] value of 77.46 ± 0.05 kJ mol^{-1} is so significantly different, despite its ambitious confidence interval. By carefully comparing their presented ion pair production spectrum (the centre-of-mass translational energy distribution at 303 V cm^{-1} as shown in Fig. 3 of their Erratum)[16] to our ion pair production threshold, the most logical explanation is that the calibration of the centre of mass translational energy distribution is much less certain than what they quote in the paper. Very accurate calibration of a VMI image is notoriously difficult to achieve and their calibration is based only on the differences of the three translational energy peaks. Because these peaks have an fwhm of more than 50 cm^{-1}, it is difficult to see how their quoted accuracy of ±8 cm^{-1} could be achieved.

5 Conclusions

By using coincidence ion pair production (cipp) spectroscopy, five high energy Rydberg states of F_2 in the 125 960–126 220 cm^{-1} range were detected. Through a simulation of the spectra and quantum defect analysis, five Rydberg states spectra were characterized and assigned (Table 1), four $^1\Sigma_u$ states and one $^1\Pi_u$ state. Furthermore, the lowest-energy Rydberg state spectrum observed (T_0 = 126 000 cm^{-1}) lacked some of the predicted rotational structure, which allowed an accurate determination of the ion pair production threshold of $15.6229_4 \pm 0.0004_3$ eV, which could be translated into an F_2 0 K dissociation energy of $1.6012_9 \pm 0.0004_4$ eV.

The F_2 0 K dissociation energy was also obtained from imaging PEPICO experiments and the derived value of $D_0 = 1.6013_2 \pm 0.0006_2$ eV is in near-perfect agreement with the cipp results. Furthermore, because the cipp and the PEPICO experiments were independently energy-calibrated based on argon and neon atomic lines, respectively, these two dissociation energy values are considered to be independently derived. Therefore, their weighted average value of $1.6013_0 \pm 0.0003_6$ eV was used to derive the fluorine atom's 0 K heat of formation ($77.25_1 \pm 0.01_7$ kJ mol^{-1}) with unprecedented accuracy.

This study shows that the novel method of coincidence ion pair production (cipp) spectroscopy can be used for the accurate detection of very high energy Rydberg states of diatomic molecules and has the potential to derive very accurate thermochemical information, *i.e.* bond energies. Further studies are needed to confirm if this mechanism also occurs in heavier halogens and whether the technique is applicable to larger molecules, as well. It is also important in this context that the F_2 molecule studied here has an ionization energy that is higher than the ion pair production threshold and, therefore, the F^+ ion signal from the ion pair production is not overwhelmed by the higher-cross section direct ionization signal from F_2^+. Formally, for an AB molecular system, the IE > E_{cipp} requirement is equivalent to EA(A) > BE(AB^+), *i.e.* the electron affinity of the A fragment is larger than the bond energy in the

molecular ion AB^+. Since the electron affinity of the fluorine atom is 3.401 eV and while the bond energy of F_2^+ is 1.601 eV, the ion pair production is possible at lower energies than F_2 ionization.

Applying this coincidence ion pair production method for both bromine and iodine, in addition to the hydrogen halides, could potentially result in new highly accurate thermochemical and spectroscopic data and state characterisation for very high energy Rydberg states. Furthermore, quantifying how these molecules can dissociate simultaneously into positive and negative ions *via* high energy radiation could have a meaningful impact on atmospheric and, especially, astrochemical studies.

Author contributions

K. Matthíasson: formal analysis, visualization, writing; Á. Kvaran: methodology, writing; G. A. Garcia: investigation, writing; P. Weidner: investigation, formal analysis, writing; B. Sztáray: investigation, formal analysis, methodology, software, writing.

Conflicts of interest

There are no conflicts to declare.

Acknowledgements

This work was funded by the National Science Foundation (grant no. CHE-1665464). Experiments were performed at the DESIRS VUV beamline of the Soleil Synchrotron under proposal numbers 20180455 and 20190866 and we thank the beamline staff for their support, in particular Dr Laurent Nahon for helpful discussions in the design and preparation of the experiment. The financial support of the University Research Fund, University of Iceland and the Icelandic Research Fund (Grant No. 184693-052) is gratefully acknowledged. We are grateful to Dr Krisztián Torma for his help with the cipp and PEPICO experiments and to Dr Branko Ruscic for fruitful conversations and running our data on top of the latest development version of the Active Thermochemical Tables.

Notes and references

1 J. L. Gole and J. L. Margrave, *J. Mol. Spectrosc.*, 1972, **43**, 65–86.
2 G. Di Lonardo and A. E. Douglas, *J. Chem. Phys.*, 1972, **56**, 5185–5186.
3 E. A. Colbourn, M. Dagenais, A. E. Douglas and J. W. Raymonda, *Can. J. Phys.*, 1976, **54**, 1343–1359.
4 V. H. Dibeler, J. A. Walker and K. E. McCulloh, *J. Chem. Phys.*, 1969, **50**, 4592–4593.
5 J. Berkowitz, W. A. Chupka, P. M. Guyon, J. H. Holloway and R. Spohr, *J. Chem. Phys.*, 1971, **54**, 5165–5180.
6 H. Nishimura, D. C. Cartwright and S. Trajmar, *J. Chem. Phys.*, 1979, **71**, 5039–5041.
7 A. P. Hitchcock, C. E. Brion, G. R. J. Williams and P. W. Langhoff, *Chem. Phys.*, 1982, **66**, 435–442.
8 R. G. Wang, Z. W. Wang, M. A. Dillon and D. Spence, *J. Chem. Phys.*, 1984, **80**, 3574–3579.
9 A. B. Cornford, D. C. Frost, C. A. McDowell, J. L. Ragle and I. A. Stenhouse, *J. Chem. Phys.*, 1971, **54**, 2651–2657.
10 A. W. Potts and W. C. Price, *Trans. Faraday Soc.*, 1971, **67**, 1242–1252.
11 H. V. Lonkhuyzen and C. A. DeLange, *Chem. Phys.*, 1984, **89**, 313–322.
12 P. M. Guyon, R. Spohr, W. A. Chupka and J. Berkowitz, *J. Chem. Phys.*, 1976, **65**, 1650–1658.
13 P. F. Levelt, K. S. E. Eikema, S. Stolte, W. Hogervorst and W. Ubachs, *Chem. Phys. Lett.*, 1993, **210**, 307–314.
14 D. C. Cartwright and P. J. Hay, *Chem. Phys.*, 1987, **114**, 305–320.
15 J. Yang, Y. S. Hao, J. Li, C. Zhou and Y. X. Mo, *J. Chem. Phys.*, 2005, **122**, 134308.
16 J. Yang, Y. S. Hao, J. Li, C. Zhou and Y. X. Mo, *J. Chem. Phys.*, 2007, **127**, 209901.
17 A. J. Yencha, D. K. Kela, R. J. Donovan, A. Hopkirk and Á. Kvaran, *Chem. Phys. Lett.*, 1990, **165**, 283–288.
18 Á. Kvaran, A. J. Yencha, D. K. Kela, R. J. Donovan and A. Hopkirk, *Chem. Phys. Lett.*, 1991, **179**, 263–267.
19 Á. Kvaran, H. Wang, G. H. Jóhannesson and A. J. Yencha, *Chem. Phys. Lett.*, 1994, **222**, 436–442.
20 Á. Kvaran, G. H. Jóhannesson and H. Wang, *Chem. Phys.*, 1996, **204**, 65–75.
21 K. P. Lawley, T. Ridley, Z. Min, P. J. Wilson, M. S. N. Al-Kahali and R. J. Donovan, *Chem. Phys.*, 1995, **197**, 37–50.
22 A. J. Yencha, T. Ridley, R. Maier, R. V. Flood, K. P. Lawley, R. J. Donovan and A. Hopkirk, *J. Phys. Chem.*, 1993, **97**, 4582–4588.
23 D. Kaur, A. J. Yencha, R. J. Donovan, Á. Kvaran and A. Hopkirk, *Org. Mass Spectrom.*, 1993, **28**, 327–334.
24 Á. Kvaran, H. Wang and G. H. Jóhannesson, *J. Phys. Chem.*, 1995, **99**, 4451–4457.
25 L. C. Zhu and P. Johnson, *J. Chem. Phys.*, 1991, **94**, 5769–5771.
26 K. Mullerdethlefs and E. W. Schlag, *Annu. Rev. Phys. Chem.*, 1991, **42**, 109–136.
27 J. D. D. Martin and J. W. Hepburn, *Phys. Rev. Lett.*, 1997, **79**, 3154–3157.
28 S. M. Poullain, K. Veyrinas, P. Billaud, M. Lebech, Y. J. Picard, R. R. Lucchese and D. Dowek, *J. Chem. Phys.*, 2013, **139**, 044311.
29 G. A. Garcia, B. K. C. de Miranda, M. Tia, S. Daly and L. Nahon, *Rev. Sci. Instrum.*, 2013, **84**, 11.
30 L. Minnhagen, *J. Opt. Soc. Am.*, 1973, **63**, 1185–1198.
31 Y. Tanaka and K. Yoshino, *J. Chem. Phys.*, 1970, **53**, 2012–2030.

32 A. Kramida and Y. Ralchenko, *JReader NIST ASD Team*, *NIST Atomic Spectra Database (version 5.8)*, National Institute of Standards and Technology, Gaithersburg, MD, 2020.

33 E. B. Saloman and C. J. Sansonetti, *J. Phys. Chem. Ref. Data*, 2004, **33**, 1113–1158.

34 F. Merkt, A. Osterwalder, R. Seiler, R. Signorell, H. Palm, H. Schmutz and R. Gunzinger, *J. Phys. B: At., Mol. Opt. Phys.*, 1998, **31**, 1705–1724.

35 NIST Chemistry WebBook, NIST (National Institute of Standards and Technology) Chemistry WebBook.

36 C. M. Pgopher Western, *A Program for Simulating Rotational, Vibrational and Electronic Spectra, University of Bristol* 2017, http://pgopher.chm.bris.ac.uk.

37 K. P. Huber and G. Herzberg, *Constants of Diatomic Molecules*, Van Nostrand-Reinhold, New York, 1979.

38 B. Sztaray and T. Baer, *Rev. Sci. Instrum.*, 2003, **74**, 3763–3768.

39 B. Sztaray, A. Bodi and T. Baer, *J. Mass Spectrom.*, 2010, **45**, 1233–1245.

40 K. Matthiasson, G. Koumarianou, M. X. Jiang, P. Glodic, P. C. Samartzis and A. Kvaran, *Phys. Chem. Chem. Phys.*, 2020, **22**, 4984–4992.

41 A. Haflidason, P. Glodic, G. Koumarianou, P. C. Samartzis and A. Kvaran, *Phys. Chem. Chem. Phys.*, 2019, **21**, 10391–10401.

42 S. X. Tian, *Phys. Chem. Chem. Phys.*, 2012, **14**, 6433–6443.

43 A. G. Suits and J. W. Hepburn, *Annu. Rev. Phys. Chem.*, 2006, **57**, 431–465.

44 B. Ruscic and D. H. Bross, *Active Thermochemical Tables (ATcT) values based on ver. 1.122p of the Thermochemical Network*, 2016.

45 W. R. Stevens, B. Ruscic and T. Baer, *J. Phys. Chem. A*, 2010, **114**(50), 13134–13145.

46 B. Csontos, B. Nagy, J. Csontos and M. Kallay, *J. Phys. Chem. A*, 2013, **117**(26), 5518–5528.

47 B. Ruscic, Private communication, 2020.

48 N. de Oliveira, M. Roudjane and D. Joyeux, *et al.*, *Nat. Photonics*, 2011, **5**, 149–153.